Spectrochimica Acta Part A: Molecular and Biomolecular Spectroscopy 98 (2012) 290–301

Contents lists available at SciVerse ScienceDirect

Spectrochimica Acta Part A: Molecular and Biomolecular Spectroscopy

journal homepage: www.elsevier.com/locate/saa

Structural, antimicrobial and computational characterization of 1-benzoyl-3-(5-chloro-2-hydroxyphenyl)thiourea

Murat Atiş [a,*], Fatma Karipcin [b], Bahtiyar Sarıboğa [b], Murat Taş [c], Hasan Çelik [b]

[a] Department of Physics, Sciences and Arts Faculty, Nevsehir University, 50300 Nevsehir, Turkey
[b] Department of Chemistry, Sciences and Arts Faculty, Nevsehir University, 50300 Nevsehir, Turkey
[c] Department of Chemistry, Sciences and Arts Faculty, Giresun University, 28100 Giresun, Turkey

HIGHLIGHTS

- The 1-benzoyl-3-(5-chloro-2-hydroxyphenyl)thiourea synthesized.
- The FT-IR, ^{13}C, ^{1}H NMR, UV spectroscopy and X-ray used for characterization.
- The B3LYP method with the standard 6-311++G(d,p) basis sets used to calculation.
- Theoretical calculations are in good agreement with experimental results.
- **Bcht** exhibited antimicrobial activity against, *Listeria monocytogenes* and *Staphylococcus aureus.*

GRAPHICAL ABSTRACT

The synthesized new thiourea derivative, 1-benzoyl-3-(5-chloro-2-hydroxyphenyl)thiourea characterized by elemental analyses, X-ray, FT-IR, ^{13}C, ^{1}H NMR, UV spectroscopy and calculated by using B3LYP method with the standard 6-311++G(d,p) basis sets; and also exhibited antimicrobial activity against, *Listeria monocytogenes* and *Staphylococcus aureus*.

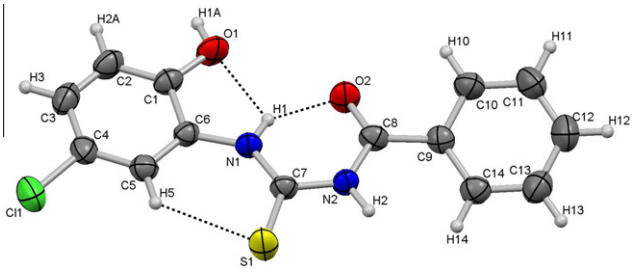

ARTICLE INFO

Article history:
Received 21 May 2012
Received in revised form 3 August 2012
Accepted 12 August 2012
Available online 20 August 2012

Keywords:
Thiourea
Spectroscopy
Crystal structure
Hydrogen bonds
DFT
Antimicrobial activity

ABSTRACT

A new thiourea derivative, 1-benzoyl-3-(5-chloro-2-hydroxyphenyl)thiourea (**bcht**) has been synthesized from the reaction of 2-amino-4-chlorophenol with benzoyl isothiocyanate. The title compound has been characterized by elemental analyses, FT-IR, ^{13}C, ^{1}H NMR spectroscopy and the single crystal X-ray diffraction analysis. The structure of **bcht** derived from X-ray diffraction of a single crystal has been presented. The structural and spectroscopic data of the molecule in the ground state were calculated by using density functional method using 6-311++G(d,p) basis set. The complete assignments of all vibrational modes were performed on the basis of the total energy distributions (TED). Isotropic chemical shifts (^{13}C NMR and ^{1}H NMR) were calculated using the gauge-invariant atomic orbital (GIAO) method. Theoretical calculations of bond parameters, harmonic vibration frequencies and nuclear magnetic resonance are in good agreement with experimental results. The UV absorption spectra of the compound that dissolved in ACN and MeOH were recorded. **Bcht** was also screened for antimicrobial activity against pathogenic bacteria and fungi.

Introduction

Thiourea derivatives are very useful building blocks for the synthesis of a wide range of aliphatic macromolecular and heterocyclic compounds [1–4]. Thioureas are potentially very versatile ligands, as they are able to coordinate to a range of metal centers as either neutral ligands, monoanions, or dianions [5–11]. In addition, the oxygen, nitrogen and sulfur donors provide a multitude of bonding possibilities. Thiourea derivatives display a wide range of biological activity including antibacterial, anti-fungal, antitubercular, antithyroid, antihelmintic, rodenticidal, insecticidal, herbicidal,

* Corresponding author. Tel.: +90 384 228 1100; fax: +90 384 215 3948.
E-mail addresses: atis@nevsehir.edu.tr, atismurat@gmail.com (M. Atiş).

1386-1425/$ - see front matter © 2012 Elsevier B.V. All rights reserved.
http://dx.doi.org/10.1016/j.saa.2012.08.020

and plant growth regulator properties [12–18]. Moreover, the hydrogen-bonding ability of the thiourea moiety has extensively been used in the construction of anion receptors [19–22] and in the thiourea-based metal complexes [7–11] and organocatalysts [23–25]. In particular, aroylthioureas have been successfully used in environmental control, as ionophores in ion selective electrodes [18,26,27].

The structure and intra-molecular and intermolecular hydrogen bonding behavior of many *N*-benzoyl-*N*′-arylthioureas have been thoroughly investigated [28–33]. In addition, the conformational changes in these molecules are analogous to those arising in folded proteins, and a full understanding of these effects requires understanding the effects of intermolecular hydrogen bonding interactions and hydrophobic interactions. The title compound can exhibit thione-thiol tautomerism because it contains a thioamide –NH–C=S functional group, and a carbonyl group, which can accept hydrogen bonding donor groups and then come into anion receptor [32].

The molecular structural study of **bcht** is important for structure-activity relationship which is useful for rational design strategy. In this present study, we have synthesized a new thiourea derivative and investigated by using FT-IR, ^{1}H NMR, ^{13}C NMR, UV spectra and X-ray crystallographic techniques in order to reveal the hydrogen bonding and tautomeric equilibrium (Scheme 1). We also report the results of calculated structure and spectra (IR, UV and NMR) of the **bcht** molecule, the calculations being on the basis of density functional theory (DFT) approximations. All spectroscopic properties which examined by the experimental techniques were supported by the computed results. In the ground state theoretical geometric parameters, IR, NMR and UV spectra and HOMO and LUMO energies of title molecule were calculated by using Gaussian 09 suite of quantum chemistry codes [34]. For **bcht**, the tautomeric thioketo-amine form is observed with C7–S1 distance of 1.660(2) Å. Strong intramolecular hydrogen bonds are found between the N1–H1···O2 atoms with an N1–H1 and N1–O2 distances of 0.86 and 2.600(2) Å.

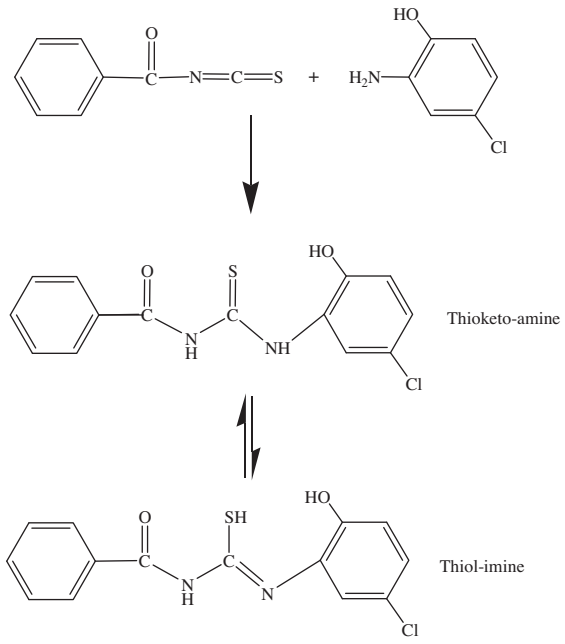

Scheme 1. Synthesis route and chemical structures of the title compound (**bcht**).

Experimental

Materials

All chemicals used for the preparation of the compound were analytically reagent grade. Acetone was dried before use.

Physical measurements

Carbon, hydrogen, nitrogen and sulfur were determined using a LECO 932 CHNS analyzer. Infrared spectrum was recorded in the 4000–650 cm^{-1} region using a Perkin Elmer Spectrum 100 FT-IR spectrometer. ^{1}H NMR and ^{13}C NMR spectra were obtained on Bruker 400 High Resolution Console in $CDCl_3$. Proton chemical shifts are reported in part per million (ppm) relative to an internal standard of Me_4Si. The UV–Visible spectra were measured using a Perkin Elmer Lambda 25 UV/VIS Spectrometer. Melting point was determined using an EZ-Melt melting point apparatus and were uncorrected.

Synthesis

1-Benzoyl-3-(5-chloro-2-hydroxyphenyl)thiourea was prepared by a procedure similar to that reported in the literature [8–11,44,45]. A solution of benzoyl chloride (2.80 g, 20 mmol) in dry acetone (10 mL) was added dropwise to a solution of NH_4SCN (1.52 g, 20 mmol) in dry acetone (30 mL) under stirring. After the addition was completed, the mixture was kept at 40 °C for 1 h, and then cooled to room temperature. The formed precipitate of NH_4Cl was filtered off. A solution of 2-amino-4-chlorophenol (2.87 g, 20 mmol) in dry acetone (20 mL) was slowly added to the resulting yellow solution, which then was stirred at ambient temperature for 2 h. Afterwards the reaction mixture was poured into ice-water mixture and stirred well. The solid product was separated and washed with deionized water, cold MeOH and diethylether and purified by recrystallization from methanol to give fine crystals of the title compound, with an overall yield of 87%.

Pale yellow crystal. Mp: 213 °C. Calcd for $C_{14}H_{11}ClN_2O_2S$: C, 54.82; H, 3.61; N, 9.13; S, 10.45%. Found: C, 55.23; H, 3.65; N, 8.80; S, 10.61%. FT-IR (cm^{-1}): ν(O–H) 3394 (m, br), ν(N–H) 3274 (m, br), ν(C–H) 3000 (m, br), ν(C=O) 1655 (s), 1598 (vs), 1524 (vs), 1486 (vs), 1426 (s), 1366 (vs), 1331 (s), 1290 (m), ν(C=S) 1253 (vs), 1185 (vs), 1142 (vs), 1079 (s), 1025 (w), 1000 (w) 980 (w), 935 (m), 871 (vs), 833 (m), 808 (vs), 707 (s), 690 (m). ^{1}H NMR ($CDCl_3$; δ, ppm): 7.00 (d, J = 8.66 Hz, 1H, Ph), 7.16 (dd, $J1$ = 8.65, $J2$ = 2.60 Hz, 1H, Ph), 7.57 (t, J = 7.88 Hz, 2H, Ph), 7.69 (t, J = 7.41 Hz, 1H, Ph), 8.00 (d, J = 7.28 Hz, 2H, Ph), 8.86 (d, J = 2.56, 1H, Ph), 10.80 (s, 1H, OH), 11.64 (s, 1H, CONH), 13.16 (s, 1H, CSNH); ^{13}C NMR ($CDCl_3$; δ, ppm): 116.2, 121.6, 122.0, 125.8, 127.2, 128.5, 128.8, 132.0, 133.3, 147.7 (Ph), 168.4 (C=O), 177.7 (C=S).

X-ray crystallographic analysis

The crystal data were collected using ω–2θ scan techniques on an Agilent SuperNova, (Single source at offset and Eos CCD detector) diffractometer with SuperNova (Mo) X-ray Source (Mo-$K\alpha$, λ = 0.71073 Å). The CrysAlisPro software program was used for data collection, cell refinement and data reduction. Using Olex2 [35], the structure was solved by the ShelXS [36] structure solution program using direct methods and refined with the ShelXL [37] refinement package using least squares minimization. To prepare material for publication Mercury 3.0 were used. All H atoms were refined using a riding model.

Computational details

All calculations were performed at density functional theory (DFT/B3LYP) at the 6-311++G(d,p) basis set level by using Gaussian 09 program [34]. Optimized structural parameters were used by in vibrational wave numbers, isotropic chemical shifts and electronic transitions calculations. The total energy distribution (TED) was calculated by using VEDA 4 [38] program. For NMR calculations, after optimization, ^{1}H and ^{13}C NMR chemical shifts (δH and δC) were calculated using the gauge-invariant atomic orbital (GIAO) method [39,40] in chloroform-*d* ($CDCl_3$) solvent. The GIAO method is one of the most common approaches for calculating nuclear magnetic shielding tensors. The GIAO approach allows the computation of the absolute chemical shielding due to the electronic environment of the individual nuclei and this method is often more accurate than those calculated with other approaches for the same basis set size. The chemical shifts were reported in ppm relative to tetramethylsilane (TMS) for ^{1}H and ^{13}C NMR spectra.

Antimicrobial studies

Bcht was screened for their antimicrobial activity against bacteria *Streptococcus pneumoniae* (ATCC 29212), *Staphylococcus aureus* (ATCC 6538), *Methicillin Resistant Staphylococcus aureus MRSA* (ATCC 43300), *Bacillus cereus* (ATCC 7064), *Entrococcus faecalis* (ATCC 29212), *Listeria monocytogenes* (ATCC 19114) and *Salmonella typhi* (CCM 5445), and *yeast. Candida albicans* (ATCC 10231) in vitro using the microdilution method. The antibacterial activity assays of all compounds were performed according to the Clinical and Laboratory Standards Institute (CLSI) protocols [41]. The antifungal activities of all compounds were evaluated according to the National Committee for Clinical Laboratory Standards (NCLS) [42]. All determinations were performed in triplicate and confirmed by three separate experiments. The MIC ($\mu g\,mL^{-1}$) was defined as the lowest concentration of compound inhibiting the growth of each strain. Vancomycine (Himedia) and Ciprofloxcacin (Sigma) for bacterial strains and Amphotericin B (Sigma) for fungal strains were used as a positive control.

Results and discussion

The synthesis of the compound involves the reaction of a benzoyl chloride with ammonium thiocyanate in dry acetone followed by condensation of the benzoyl isothiocyanate with 2-amino-4-chlorophenol. The compound was purified by recrystallisation from methanol and characterized by elemental analysis, ^{1}H, ^{13}C NMR, UV, IR spectroscopy and the single crystal X-ray diffraction analysis. **Bcht** is insoluble in water, ether, and hexane but slightly soluble in chloroform, methanol, and ethanol and soluble in DMF, DMSO, ACN and acetone. The analytical and spectroscopic data are consistent with the structures given in Fig. 1.

Description of the crystal structure

The structure of 1-benzoyl-3-(5-chloro-2-hydroxyphenyl)thiourea was confirmed by the result of a single crystal X-ray structure determination. Fig. 1 shows the molecular structure of **bcht**. Experimental details for data collection and structure refinement are summarized in Table 1. The selected bond lengths and angles are presented in Table 2 (includes intra and inter molecular interactions).

In **bcht**, the bond lengths and angles are generally normal in the *N*-alkyl-*N*′-benzoylthiourea compounds [4,31–33,43,44]. The bond lengths of the carbonyl (C8–O2 = 1.230(2) Å) and thiocarbonyl (C7–S1 = 1.660(2) Å) groups of **bcht** have typical double-bond character [31–33,43,44]. However, the C–N bond lengths for the investigated compound are all shorter than the average single C–N bond length of 1.472(5) Å, being C7–N2 = 1.403(2) Å, C8–N2 = 1.368(2) Å, C6–N1 = 1.402(2) Å, C7–N1 = 1.327(2) Å thus showing varying degrees of single bond character [4,31–33,43,44]. Bond characters of the structure are presumed as a result of the intra-molecular H-bond "locking" the molecule into a planar six-numbered ring structure. These results are in agreement with the expected delocalization in **bcht** and confirmed by C8–N2–C7 = 128.52(17)° and C7–N1–C6 = 132.58(17)° angles showing a sp^2 hybridization on the N1 and N2 atoms. As presented in Fig. 1, the molecule maintains its *cis–trans* configuration with respect to the position of the phenyl and 2-hydroxo-5-chlorophenyl groups relative to the thiocarbonyl sulfur atom across the N2–C8 and N1–C7 bonds, respectively [43,44]. The conformation of the molecule with respect to the thiocarbonyl and carbonyl moieties is twisted, as reflected by the torsion angles C7–N2–C8–O2, C8–N2–C7–N1 and C8–N2–C7–S1 −4.1(3), 3.5(3) and −175.80(17), respectively.

The phenyl rings are nearly planar and the angle between the two phenyl ring planes is found as 18.25°. The angles between the planes forming by C8–N2–C7–N1–S1–O2 atoms are calculated as 2.92° and 20.04° for 2-hydroxy-4-chlorophenyl ring plane and for the other phenyl ring plane, respectively. These results indicated that the phenyl rings were twisted around the non-aromatic part of the compound and this may attribute to the intra molecular hydrogen bond between the the C5 atom of 2-hydroxy-4-chlorophenyl part and ticketing part.

As presented in Table 2 and Fig. 1, the N1 atom formed bifurcated intramolecular hydrogen bonds with the carbonyl oxygen (O2) and hydroxyl oxygen (O1). The C5 atom of a phenyl group formed an intramolecular hydrogen bond with sulfur atom of the compound.

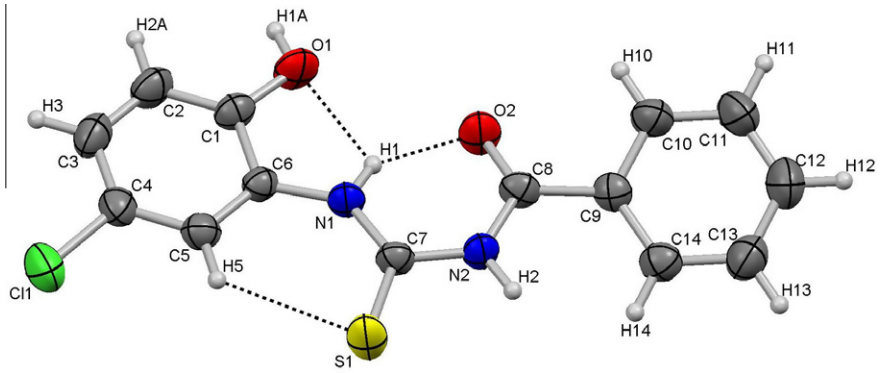

Fig. 1. The intramolecular H-bonds and the structure diagram with 50% probability ellipsoids of the compound with atomic numbering scheme.

Table 1
Crystal data and structure refinement for **bcht**.

Identification code	H1_5
Empirical formula	$C_{14}H_{11}ClN_2O_2S$
Formula weight	306.76
Temperature/K	293 (2)
Crystal system	Monoclinic
Space group	$P2_1/n$
a/Å	11.1594 (6)
b/Å	4.7461 (3)
c/Å	25.8628 (13)
α/°	90.00
β/°	98.484 (5)
γ/°	90.00
Volume/Å^3	1354.80 (13)
Z	4
ρ_{calc}mg/mm^3	1.504
m/mm^{-1}	0.438
$F(000)$	632.0
Crystal size/mm^3	0.128 × 0.143 × 0.218
2Θ range of data collection	6.46 to 74.84°
Index ranges	$-17 \leqslant h \leqslant 18$, $-3 \leqslant k \leqslant 8$, $-43 \leqslant l \leqslant 27$
Reflections collected	11552
Independent reflections	6738[R(int) = 0.0467]
Data/restraints/parameters	6738/0/182
Goodness-of-fit on F^2	1.019
Final R indexes [I> = 2σ (I)]	R_1 = 0.0662, wR_2 = 0.1184
Final R indexes [all data]	R_1 = 0.1736, wR_2 = 0.1661
Largest diff. peak/hole/e Å^{-3}	0.27/−0.35

The molecules extended by the intermolecular hydrogen bonds are given in Table 2 and showing in Fig. 2 to form two dimensional networks along the *b* and *c* axes. The interactions presenting in Fig. 3 extend the molecules along the axis. So, the molecules form three dimensional networks of intermolecular hydrogen bond and C–O···π interactions (Fig. 4).

The calculated bond parameters are also listed in Table 2. The optimized structural parameters of title compound were calculated at B3LYP/6-311++G(d,p) basis set level. The correlation between the experimental and calculated geometric parameters obtained by the DFT methods is given in Table 2. The bond lengths are well correlated by cross 0.9879 with observed data. The differences between calculated and observed bond lengths of hydrogen (X–H) are higher than bond non-contain hydrogen. For example, the correlation values between calculated and experimental are 0.9895, 0.9914 and 0.9965 for CC, NC and CO, respectively. However, they are 0.8584, 0.8444 and 0.8524 for CH, NH and OH, respectively. Arslan et al. [45] reported that DFT method correlates (r = 0.9952) well for the bond length compared with the HF method. Also, their [45] largest difference between experimental and calculated DFT bond length is about 0.047 Å while it is 0.154 for X–H and 0.019 Å for X–X bonds in the present study, respectively. As a result, the optimized bond lengths obtained by DFT-B3LYP/6-311++G (d,p) method shows the best agreement with the experimental values. The difference between experimental and calculated geometric parameters comes from the environment of the compound. It is clear that the experimental results belong to solid phase and theoretical calculations belong to a gaseous phase.

FT-IR spectrum

The experimental and theoretical Infrared spectra of **bcht** are shown in Fig. 5, where calculated intensity is plotted against the wave numbers. The observed and calculated wave numbers along with their relative intensities and probability assignments with TED of title molecule are given in Table 3. The theoretical calculations were made for a free molecule of vacuum, while the experiments were performed for the solid sample. Therefore, there are

Table 2
Selected bond lengths (Å), Angels, Torsion angles (Å) and interactions for **bcht**.

Bond length	XRD	Calc.	Bond angle	XRD	Calc.	Dihedral angle	XRD	Calc.
S1–C7	1.660(2)	1.673	C10–C9–C8	116.78(19)	117.14	N1–C6–C1–C2	−179.48(19)	−179.24
Cl1–C4	1.736(2)	1.760	C14–C9–C8	124.10(19)	123.49	N1–C6–C1–O1	0.7(3)	0.81
N2–C7	1.403(2)	1.409	O2–C8–C9	120.48(18)	121.84	N1–C6–C5–C4	−179.83(19)	−179.14
N2–C8	1.368(2)	1.382	N2–C8–C9	118.18(17)	115.67	N2–C8–C9–C10	−160.9(2)	−159.05
O2–C8	1.230(2)	1.225	O2–C8–N2	121.33(19)	122.48	N2–C8–C9–C14	17.7(3)	22.44
N1–C6	1.402(2)	1.408	C8–N2–C7	128.52(17)	130.45	O2–C8–C9–C10	17.8(3)	20.28
N1–C7	1.327(2)	1.349	N1–C7–S1	127.53(16)	129.46	O2–C8–C9–C14	−163.6(2)	−158.22
O1–C1	1.355(2)	1.368	N1–C7–N2	114.86(16)	114.28	C6–N1–C7–N2	−178.58(19)	−178.70
C6–C5	1.378(3)	1.397	N1–C6–C1	113.45(18)	115.27	C6–N1–C7–S1	0.6(3)	1.53
C6–C1	1.405(3)	1.412	N2–C7–S1	117.60(14)	116.26	C7–N1–C6–C1	176.9(2)	175.08
C5–C4	1.383(3)	1.391	C5–C6–N1	127.08(17)	126.00	C7–N1–C6–C5	−3.0(4)	−5.76
C8–C9	1.481(3)	1.497	C7–N1–C6	132.58(17)	131.22	C7–N2–C8–C9	174.61(18)	176.80
C1–C2	1.374(3)	1.387	O1–C1–C6	115.87(18)	116.27	C7–N2–C8–O2	−4.1(3)	−3.87
C9–C14	1.385(3)	1.401	O1–C1–C2	124.23(19)	123.16	C8–N2–C7–N1	3.5(3)	−0.81
C9–C10	1.391(3)	1.400	C5–C6–C1	119.47(19)	118.73	C8–N2–C7–S1	−175.80(17)	−179.39

Hydrogen bond geometries

D–H···A	D–H	H···A	D···A	D–H···A
N1–H1···O2	0.86	1.86	2.600(2)	142.9
N1–H1···O1	0.86	2.09	2.555(2)	113.2
C5–H5···S1	0.93	2.58	3.225(2)	127.1
N2–H2···S1^{i}	0.86	2.83	3.6027(17)	150.4
C14–H14···S1^{i}	0.93	2.78	3.368(2)	122.4
O1–H1A···O2^{ii}	0.82	1.95	2.762(2)	171.1
C2–H2A···O2^{ii}	0.93	2.92	3.543(3)	125.5
C13–H13···S1^{iii}	0.93	3.07	3.857(3)	143.1
C11–H11···Cl1^{iv}	0.93	3.04	3.675(3)	127.2
C11–H11···Cl1^{v}	0.93	3.05	3.642(3)	123.1

C–O···π interactions geometries

C8–O2···Cg1^{vi}	1.230(2)	3.8924(18)	4.096(2)	90.67(12)
C8–O2···Cg2^{vii}	1.230(2)	3.8309(18)	3.721(2)	75.59(11)

i = −x, 1−y, −zii = 1/2−x, −1/2 + y, 1/2−ziii = −x,2−y, −ziv = 1 + x,1 + y,ziv = 1x,2 + y, zvi = x,1 + y, zvii = x, −1 + y, z

Cg refer to center of the rings Cg1 for C1–C2–C3–C4–C5–C6 Cg2 for C9–C10–C11–C12–C13–C14

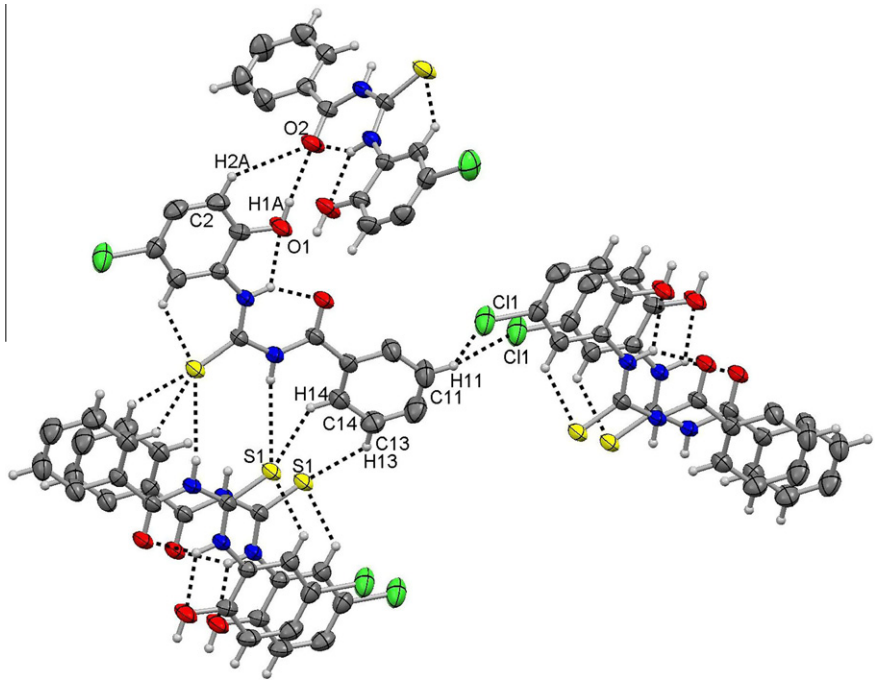

Fig. 2. Inter-molecular hydrogen bonds interactions.

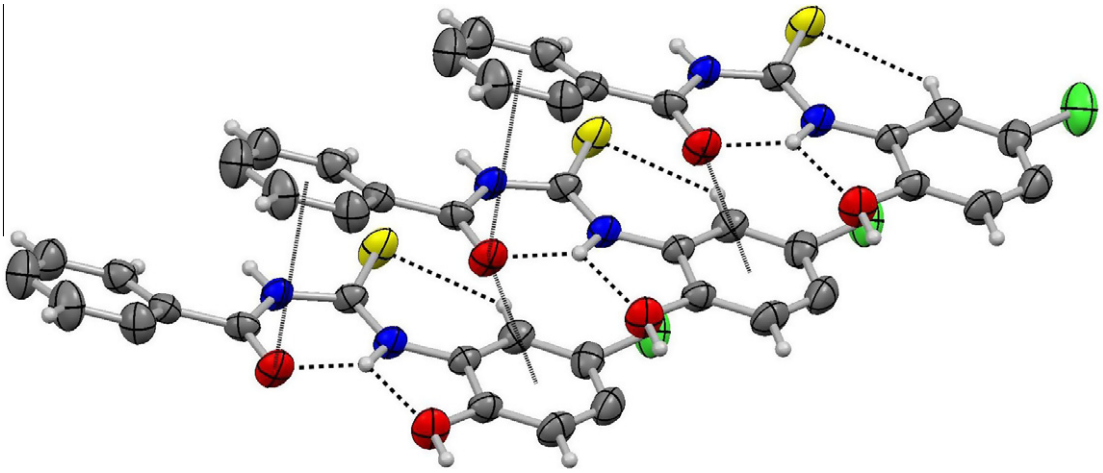

Fig. 3. C–O···π interactions.

nonsignificant disagreements between them. The title compound contains 31 atoms, and so they have 87 normal vibrational modes. The optimized geometry was used for vibrational analysis calculation. Because there was no imaginary frequency for the stationary points, the optimized structure accepted as real minimum. Vibrational spectral assignments have been performed on the recorded FT-IR spectrum based on theoretically predicted wavenumbers and their TED.

The vibrational wavenumbers were crossed with a uniform scaling factor for agreement with experimental data well. The calculated wavenumbers are usually higher than the corresponding experimental quantities because of the combination of electron correlation effects and basis set deficiencies. The observed slight disagreement between theory and experiment could be a consequence of the anharmonicity and the general tendency of the quantum chemical methods to overestimate the force constants at the exact equilibrium geometry. Therefore, it is customary to scale down the calculated harmonic wavenumbers in order to improve the agreement with the experiment. In our study, we have followed two different scaling factors, i.e. 0.983 up to 1700 cm^{-1} and 0.958 for <1700 cm^{-1} [46].

The band at 3394 cm^{-1} should be attributed to the stretching frequencies of the O–H group. Medium peak at 3274 cm^{-1} is attributed to the stretching vibration of N–H groups. The appropriate calculated frequencies of νOH and νNH are positioned at 3688 and 3462 cm^{-1}, respectively when DFTB3LYP/6-311++G(d,p) method was applied. The TED contribution of these stretching modes indicates that these are pure stretching modes. The difference between experimental and calculated νOH and νNH are about 294 and 188 cm^{-1}, respectively. This striking discrepancy comes from the formation of intermolecular hydrogen bonding with O–H and N–H. Also, we note that the experimental results belong to solid phase and theoretical calculations belong to a gaseous phase.

In aromatic compounds the νCH, βCH and γCH modes are appearing in the range of 3000–3100, 1000–1300 and 750–1000 cm^{-1}, respectively [47,48]. In this study, towards the end the last six

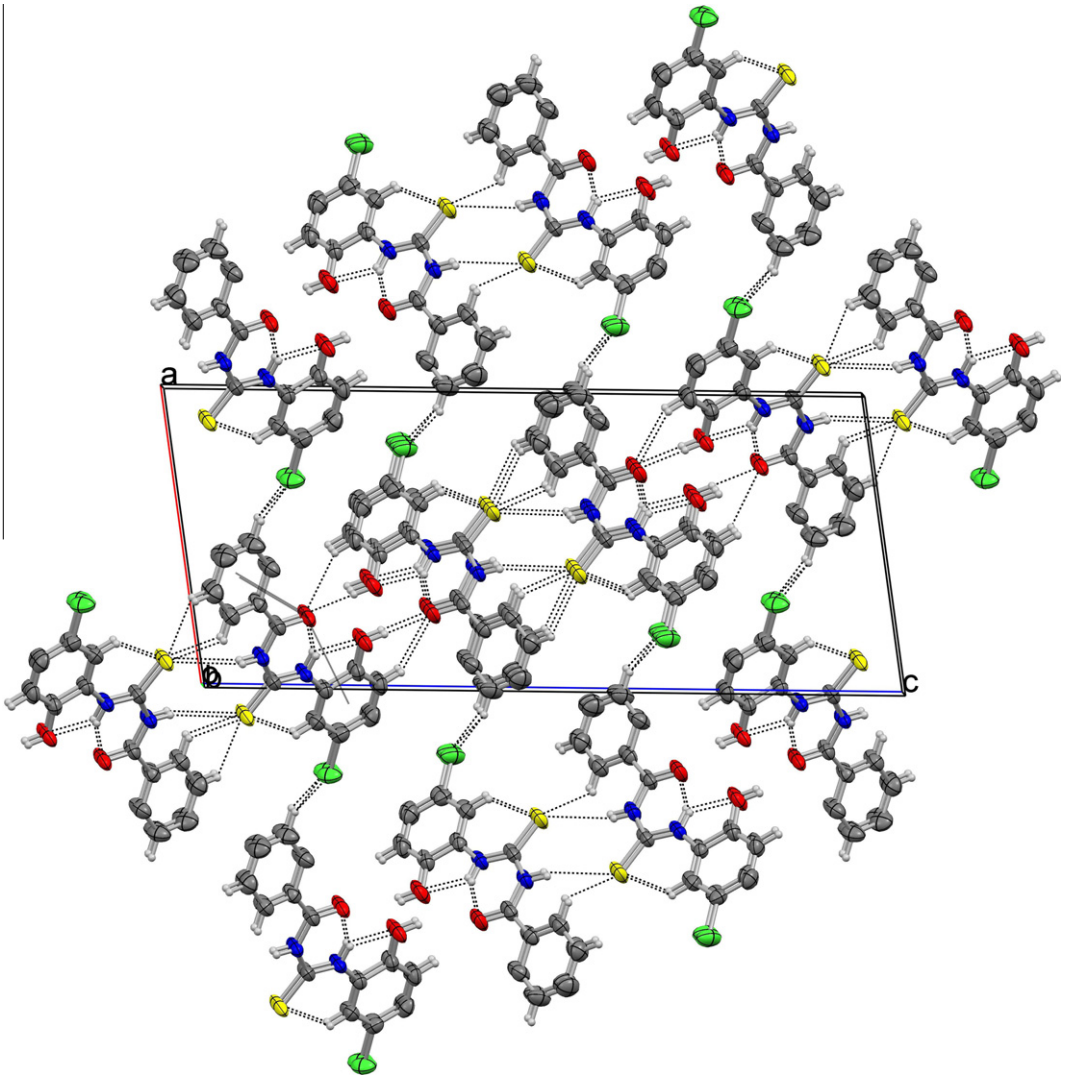

Fig. 4. A view of packing diagram of the synthesized compound.

vibrations are assigned to C–H stretching, which correspond to stretching modes C–H of ring units. All modes are nearly pure stretching vibrations 100% TED terms. The experimental C–H stretching vibrations appeared at 3000 cm^{-1}. The C–H in-plane bending vibrations appeared in the range 1084–1333 cm^{-1} and their corresponding experimental wavenumbers, 980–1331 cm^{-1} are inconsistent with computed values. According to their TED, they are described as mixed modes, generally with C–C stretching vibrations. The assignments also find support from the literature [48–50].

The νCH stretching vibrations of the phenyl ring were assigned to a band observed at 3000 cm^{-1} in the IR spectrum of **bcht**. The difference between experimental and calculated νCH is about 29 cm^{-1}. The bigger differences belong to stretching vibrations of C–H bond forming intermolecular hydrogen bonding.

Stretching vibration of carbonyl group C=O can be observed as a very strong band in both FT-IR at 1655 cm^{-1}. The carbonyl stretching C=O vibration is expected to occur in the region 1715–1680 cm^{-1} [48,51]. This is interpreted by the result of its conjugated resonance with the phenyl ring and by the formation of intra-molecular hydrogen bonding with N–H. The difference between experimental (1655 cm^{-1}) and calculated (1649 cm^{-1}) νC=O is about 6 cm^{-1}.

The ring carbon-carbon stretching vibrations are appearing in the range of 1625–1430 cm^{-1}. In general, the bands are of variable intensity and are observed at 1625–1590, 1590–1575, 1540–1470, 1460–1430 and 1380–1280 cm^{-1} from the wavenumber ranges reported by Varsanyi [52] for the five bands in the region. In the present work, the wavenumbers assigned in the FT-IR spectrum at 1598, 1426, 1331–1290, 1253 and 1185–1141 cm^{-1} are assigned to C–C stretching vibrations. The symmetric ring-breathing mode was usually found to be near 1000 cm^{-1} in the monosubstituted benzene ring. The bands at 1025–871 cm^{-1} should be attributed to the vibration of ring-breathing. Shimanouchi et al. [53] reported the wavenumber data of these vibrations in different benzene derivatives through normal coordinate analysis. The band observed at 689 cm^{-1} in the FT-IR spectrum is assigned to C–C–C deformation of the phenyl ring. The same vibration appears in the theoretical calculation at 682 cm^{-1}. The TED contribution of this mode (17%) indicates that this is a pure mode.

The abnormally intense absorption peak at 1524 cm^{-1} is regarded as the asymmetric stretching vibrations of N–C–N. It reveals that intra-molecular hydrogen bonding exists in the compound.

The identification of other C–N vibration is a very difficult task, since the mixing of several bands is possible in this region. However, with the help of theoretical calculation (DFT), the C–N stretching vibrations are calculated. The C–N stretching vibration coupled with scissoring of N–H and C–C is moderately to strongly

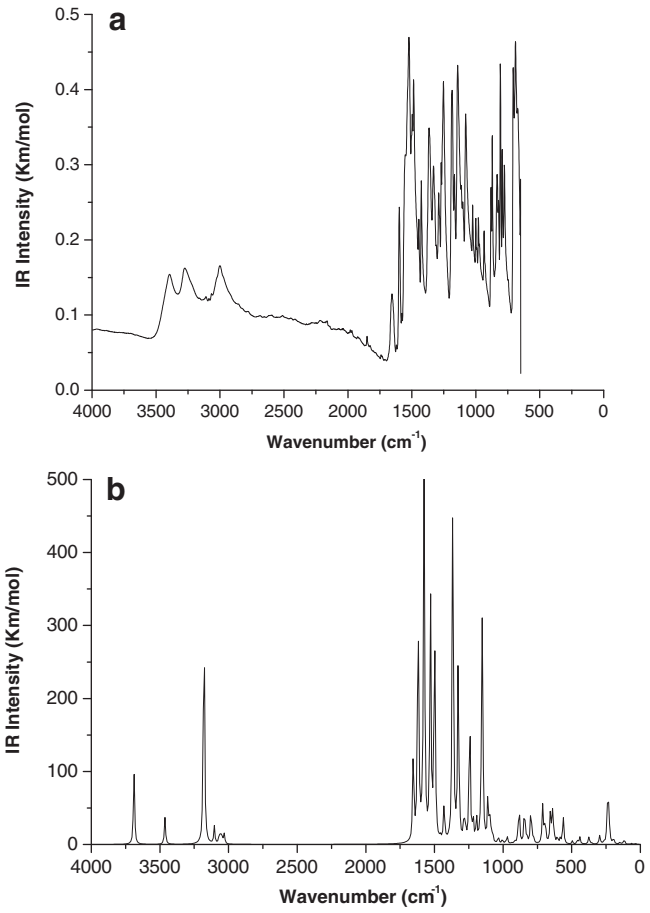

Fig. 5. (a) Experimental and (b) Theoretical IR spectra of 1-benzoyl-3-(5-chloro-2-hydroxyphenyl)thiourea.

active in the region 1275 ± 55 cm^{-1} [51]. In the present investigation C–N stretching frequencies are observed at 1079, 1185, 1253, 1331 and 1366 cm^{-1} by FT-IR and their corresponding calculated wavenumbers appeared in the range of 1146–1361 cm^{-1}. These experimental values of C–N stretching mode show good agreement with theoretical values. The νCN stretching vibration normally appears around 1300 cm^{-1} [48,51].

The band at 1253 cm^{-1} might be attributed to ν(C–O). The recorded four peaks by Klots et al. [54] which are 608.8, 753.5, 839.5, and 872.8 cm^{-1} are assigned to C–S stretching by Singh et al. [55] according to the potential energy distribution (PED) obtained from DFT calculations. In this study, we have assigned five bands due to the C–S stretching based on the TED calculations, and obtained a single band at 773 cm^{-1} (mode 35) which the observed value is 707 cm^{-1}. In this study, two in-planes bending of S–C–N calculated at 222 and 233 cm^{-1} and an out-plane-bending of S–N–N–C calculated at 598 cm^{-1} based on TED calculation. The IR spectrum of the compound does not display the S–H mode at about 2600 cm^{-1} indicating that in the solid state this compound remains in the thioketo-amine form [32,33,56,57]. The non-discussed modes details are given in Table 3. The majority of the experimental FT-IR values show good agreement with theoretical values.

NMR spectra

The NMR spectrum was recorded in $CDCl_3$ at room temperature at 400.00 MHz on a Bruker 400 instrument. The two most deshielded signals were assigned to NH protons. The NMR data are shown in Table 4. The atom positions were numbered in Fig. 1. The NMR spectrum is recognized that accurate predictions of molecular geometries are essential for reliable calculations of magnetic properties. Therefore the molecular structure of title compound was optimized before theoretical NMR calculation. Then, gauge-including atomic orbital (GIAO) ^{13}C NMR and ^{1}H NMR chemical shift calculations were carried out by using B3LYP functional with 6-311++G(d,p) basis sets. The GIAO [39,40] method is one of the most common approaches for defining isotropic nuclear magnetic shielding tensors. For the same basis set size, the GIAO method is often more accurate than other approaches [58]. The calculations reported were performed in $CDCl_3$ solution using the IEF-PCM model, rather than in the gas phase, in agreement with experimental chemical shifts obtained in $CDCl_3$ solution. The isotropic shielding values were used to calculate the isotropic chemical shifts with respect to tetramethylsilane (TMS). As seen from Table 4, experimental and theoretical results are generally in good agreement. However, all of the theoretical ^{13}C NMR values a bit bigger from observed values. But in ^{1}H NMR values, there is not any systematic relation between experimental and calculated values. While some theoretical ^{1}H NMR values have perfect agreement (like as H1, H2A, H3, H14), some values are so different (like as H2 and H1A), (Table 4).

Corresponding to the literature, the ^{1}H NMR spectrum of **bcht** indicates that the NH resonances appear at 13.16 and 11.64 ppm, but these resonances vary with different parameters, such as the substituted groups on the rings, which release and withdraw electron density in each ring, their positions and intra- and intermolecular hydrogen bondings [32,57,59]. In most compounds with aromatic substituent at N1, the hydrogen bonded proton N1–H1 has a higher δ ^{1}H value between 12 and 13 ppm. Acidic protons N2–H2 show their δ ^{1}H values between 11 and 12 ppm. ^{1}H NMR studies in $CDCl_3$ show that the proton of N1–H1 chemical shift is found about δ 13.16 ppm for the hydrogen bonded proton N1–H1. The chemical shift of acidic proton of N2–H2 is about δ 11.64 ppm. The chemical shift of proton of O1–H1A is about δ 10.80 ppm. The protons at benzene ring resonance come out in downfield at about δ 7.0–8.86 ppm. This can be corroborated with concrete examples: The protons H14–H10, δ = 8.00 ppm (d, 2H, J = 7.28 Hz), appear in downfield due to intra-molecular hydrogen bonded reaction O2···H14 and H10. The protons H13 and H11 appear at δ = 7.57 ppm (t, 2H, J = 7.88 Hz), the proton H12 appears at δ = 7.69 ppm (t, 1H, J = 7.41 Hz), the protons H5, H3, H2A appear at 8.86 (d, 1H, J = 2.56 Hz), 7.16 (dd, 1H, J = 2.60, 8.65 Hz), 7.00 (d, 1H, J = 8.66 Hz) ppm, respectively, in light of substituted group effect.

The most de-shielded ^{13}C NMR signals correspond to C=O and C=S groups. The carbon atom of thiocarbonyl group δ 177.7 ppm shows the highest values, due to the lower excitation energy n–π^* [60]. The ^{13}C NMR signals of carbonyl group appearing at δ 168.4 ppm are more de-shielded in the NMR spectra, due to the existence of the intra-molecular hydrogen bond related to the carbonyl oxygen atom. Meanwhile, the aromatic carbon resonances can be found in between δ_C 116.2–147.7 ppm which is corresponding to phenyl rings in the compound. This similar chemical shift could be due to the isolated position of the thione group in these compounds [32,43,57,61].

HOMO, LUMO analysis

The highest occupied molecular orbital (HOMO) energy and the lowest unoccupied molecular orbital (LUMO) energy and the energy gap of HOMO and LUMO for **bcht** calculated at the B3LYP/6-311++G(d,p) level is shown in Table 5. Both HOMO and LUMO play an important role in the electrical and optical properties, as well as in UV–Vis spectra and chemical reactions [62–64]. The bioactivity and chemical activity of the molecule depends on the eigenvalue of

Table 3
Comparison of the theoretical and experimental vibrational spectra and proposal assignment.[a]

No	IR_{Exp}	IR_{Calc}			TED (⩾10%)
		Unsc.	Sc.	IR_{int}	
1		10	10	0.07	τCCNC(70), CNCN(17)
2		27	27	1.26	τCCNC(10), NCCC(21), CNCC(40), CNCN(16)
3		40	39	0.25	τNCCC(51), CNCC(16)
4		57	56	1.21	βNCN(14), NCC(16), CNC(36)
5		84	83	0.00	τCCCN(19), NCNC(29), CNCN(14)
6		110	109	6.75	τCCCN(10), NCNC(34), CNCN(12)
7		124	122	0.02	τCCCC(54) + γClCCC(25)
8		124	122	0.95	βCCN(23), CNC(11), ClCC(13)
9		144	141	2.91	βNCN(21)
10		191	188	7.87	τCCCC(20) + γCCCC(18)
11		226	222	54.66	βSCN(21) + τHOCC(44)
12		237	233	45.96	βSCN(21) + τHOCC(42)
13		263	258	2.47	τCCCN(14), CNCN(18) + γClCCC(18)
14		286	281	0.97	βCNC(11), CCC(17), ClCC(24)
15		295	290	12.06	βOCC(15), CCC(21), ClCC(23)
16		353	347	1.34	τCCCC(33), CCCN(10) + γClCCC(17), OCCC(23)
17		373	367	11.24	βOCN(21), NCN(14), CNC(19)
18		380	374	0.62	νClC(39) + βCCC(15)
19		410	403	0.25	τ HCCC(11), CCCC(49)
20		417	410	0.06	νCC(15) + βCCC(14) + τCCCC(10)
21		441	434	10.06	βOCC(12) + τCCCC(14) + γCCCC(12)
22		460	452	5.91	τHCCC(20), CCCC(35) + γOCCC(28)
23		497	489	4.26	βNCC(11), OCC(21)
24		565	555	41.64	βCCC(12), NCC(16), OCC(14)
25		587	577	6.58	τHCCC(11), CCCN(38) + γClCCC(22)
26		608	598	9.17	τHNCC(11) + γSNNC(69)
27		631	620	4.36	βCCC(67) + τHNCC(10)
28		636	625	12.89	βCNC(10) + τHNCC(15)
29		646	635	43.78	τHNCC(53)
30		661	649	38.65	βCCC(17)
31	689	694	682	11.26	βCCC(17)
32	689	701	689	18.37	τCCCC(68)
33	689	716	704	55.76	τHCCC(24) + γONCC(32)
34	707	727	714	1.07	τHCCC(12), CCCC(54) + γOCCC(15)
35	707	786	773	8.61	νSC(36)
36	707	803	790	38.50	τHCCC(76) + γOCCC(16)
37	777	808	794	13.66	τHCCC(12), CCCC(10) + γONCC(27), CCCC(17)
38	793	835	821	9.59	νOC(13) + βCCC(34)
39	808	852	838	50.71	τHNCN(84)
40	808	858	843	0.95	τHCCC(98)
41	808	892	876	46.09	βOCN(18), CNC(11)
42	822	900	884	11.38	τHCCC(70)
43	822	924	909	3.47	τHCCC(85), CCCC(11)
44	833	947	931	0.96	τHCCC(80)
45	833	981	964	10.91	βCCC(33), NCN(11)
46	871	995	978	1.18	τHCCC(89)
47	871	1013	996	0.31	τHCCC(80)
48	871	1016	999	5.43	νCC(21) + βCCC(62)
49	881	1047	1029	8.95	νCC(41) + βCCC(11)
50	935	1089	1070	13.57	νCC(10), NC(30)
51	980	1103	1084	13.15	νCC(39) + βHCC(16)
52	1000	1109	1091	23.93	νCC(25) + βHCC(28)
53	1025	1123	1104	63.89	νCC(12) + βCCC(11), HOC(17), HCC(11)
54	1079	1165	1146	306.38	νNC(40) + βHNC(10)
55	1141	1177	1157	32.00	νCC(13) + βHOC(29), HCC(41)
56	1167	1186	1166	0.97	νCC(10) + βHCC(74)
57	1185	1208	1188	32.33	νCC(12) + βHCC(64)
58	1185	1234	1213	32.12	νNC(31) + βCCC(10)
59	1253	1259	1237	193.69	νCC(21) + βHNC(14)
60	1253	1293	1271	26.98	νCC(15), OC(26) + βHCC(20)
61	1271	1303	1281	21.79	βHCC(44)
62	1290	1335	1313	13.91	νCC(41)
63	1331	1345	1322	238.52	νCC(24), NC(11) + βHOC(12)
64	1331	1356	1333	5.18	νCC(11) + βHCC(61)
65	1366	1384	1361	511.06	νNC(25)
66	1426	1449	1424	56.00	νCC(53) + βHCC(15)
67	1445	1477	1452	4.74	βHCC(53)
68	1486	1518	1492	247.57	βHNC(11), HCC(12)
69	1497	1525	1499	71.03	βHCC(30)
70	1524	1551	1524	342.36	νNC(13) + βHNC(44)
71	1598	1598	1570	546.39	νCC(14) + βHNC(35)
72	1598	1619	1591	14.59	νCC(41)
73	1598	1640	1612	30.55	νCC(39)

(*continued on next page*)

Table 3 (*continued*)

No	IR_{Exp}	IR_{Calc}			TED (⩾10%)
		Unsc.	Sc.	IR_{int}	
74	1598	1640	1612	110.28	νCC(39)
75	1598	1643	1616	224.35	νCC(12) + βHNC(24)
76	1655	1721	1649	129.23	νOC(70) + βHNC(10)
77	3000	3161	3029	11.12	νCH(97)
78	3000	3165	3032	3.71	νCH(96)
79	3000	3172	3039	1.82	νCH(96)
80	3000	3183	3050	12.63	νCH(86)
81	3000	3194	3059	11.83	νCH(81)
82	3000	3204	3070	5.39	νCH(97)
83	3000	3208	3073	0.55	νCH(97)
84	3000	3238	3102	24.00	νCH(99)
85	3274	3317	3178	348.00	νNH(99)
86	3274	3614	3462	38.21	νNH(100)
87	3394	3850	3688	99.91	νOH(100)

[a] Unsc. – Unscaled, Sc. – Scaled, IRint – IR intensity (Kmmol^{-1}), ν-streching; β-in-plane-bending; γ-out-of-plane bending; τ-torsion. TED ⩾ 10% are shown.

Table 4
The experimental and predicted ^{13}C and ^{1}H isotropic chemical shifts (with respect to TMS, all values in ppm) for 1-benzoyl-3-(5-chloro-2-hydroxyphenyl)thiourea.

Atom	Exp.	B3LYP	Atom	Exp.	B3LYP
C7	177.8	186.34	H1	13.16	13.12
C8	168.4	171.62	H5	8.86	10.21
C1	147.7	152.05	H2	11.64	8.88
C12	133.3	140.85	H10	8.00	8.59
C4	132.0	139.82	H14	8.00	8.04
C9	127.2	139.15	H12	7.69	7.91
C10	128.5	137.31	H11	7.57	7.89
C11	128.8	135.95	H13	7.57	7.85
C13	128.8	135.32	H3	7.16	7.19
C6	125.8	134.09	H2A	7.00	6.94
C14	128.5	132.06	H1A	10.80	4.83
C3	122.0	131.45		–	–
C5	121.6	125.64		–	–
C2	116.2	118.67		–	–

Table 5
Calculated energy values of 1-benzoyl-3-(5-chloro-2-hydroxyphenyl)thiourea in its ground state with singlet symmetry and dipole moment at DFT method in the gas phase.

TD-DFT/B3LYP/6–311++G (d, p)	
Energy (eV)	GAS
HOMO	−6.147
LUMO	−2.294
HOMO–LUMO gap, (δE)	−3.853
HOMO−1	−6.294
LUMO + 1	−1.339
HOMO–LUMO gap, (δE)	−4.954
Dipole moment, μ(D)	−6.147
Symmetry	C1

HOMO, LUMO and energy gap. The HOMO represents the ability to donate an electron, LUMO as an electron acceptor represents the ability to obtain an electron. This electronic absorption corresponds to the transition from the ground to the first excited state and is mainly described by one electron excitation from the HOMO to the LUMO. The smaller the energy gap of LUMO and HOMO, the easier it is for the electrons of HOMO to be excited. The higher the energies of HOMO, the easier it is for HOMO to donate electrons; the lower the energies of LUMO, the easier it is for LUMO to accept electrons [64,65]. From the molecular orbital analysis the energy difference between the HOMO and LUMO is about −3.853 eV. The frontier molecular orbital of **bcht** (HOMO–LUMO) is shown in Fig. 6.

$$\text{HOMO energy(B3LYP)} = -6.147\text{eV}$$

$$\text{LUMO energy (B3LYP)} = -2.294\text{eV}$$

$$\text{HOMO} - \text{LUMO energy gap (B3LYP)} = -3.853\text{eV}$$

The calculated self-consistent field (SCF) energy of **bcht** is −1658.757 a.u. The HOMO and LUMO energy gap explains the eventual charge transfer interactions taking place within the molecule. The smaller band gap energy increases the stability of the molecule [64].

In the ground state, the charge density is mainly accumulated on the 5-chloro-2-hydroxyphenyl ring and C═S parts in the case of HOMO. The charge densities move to benzoyl group in case of LUMO. The charge density of the HOMO orbitals allows to visually considering the most probable sites for an interaction with nucleophilic species. In this case, the nitrogen and sulfur atoms are surrounded by a greater surface of negative charge, becoming these sites potentially more favorable for a possible coordination point. On the other hand, it was found that there are other effects such as the formation of a hydrogen bridge that could be playing in favor of the six member heterocyclic ring formation, making impossible the simultaneous coordination with the sulfur and an oxygen atom of the carbonyl group [66].

Another electronic effect that accentuates the nucleophilic regioselectivity through the sulfur atom, is the formation of resonant bonds in the 6 member ring, specifically the (O)C–N- and (S)C–N bonds, corroborated with the bond length, which is shorter than in a normal C–N bond, about 1.47 Å [4,31–33,43,44]. In this type of bonds, it does not occur any rotation in the molecule at the same level due to the rigidity provided by the electronic distribution of nature π bond [66].

Electronic spectra

Electronic absorption spectra of **bcht** were recorded in the 200–400 nm range in ACN and methanol. Absorption bands in ACN were observed at 239, 266 and 328 nm in UV region of the intraligand charge transfer transitions π–π*(phenyl nucleus) and *n*–π*, (C═N/(C═S and C═O). In order to explain the electronic transition and to compare with the experimental spectrum, TD-DFT method was applied to obtain a prediction of the electronic spectrum based on the B3LYP/6-311++G(d,p) level optimized structure. The solvent effect of the theoretical electronic transitions was studied with the PCM (polarized continuum model) in ACN. The experimental and computed electronic values, such as absorption wavelength, excitation energies, and oscillator

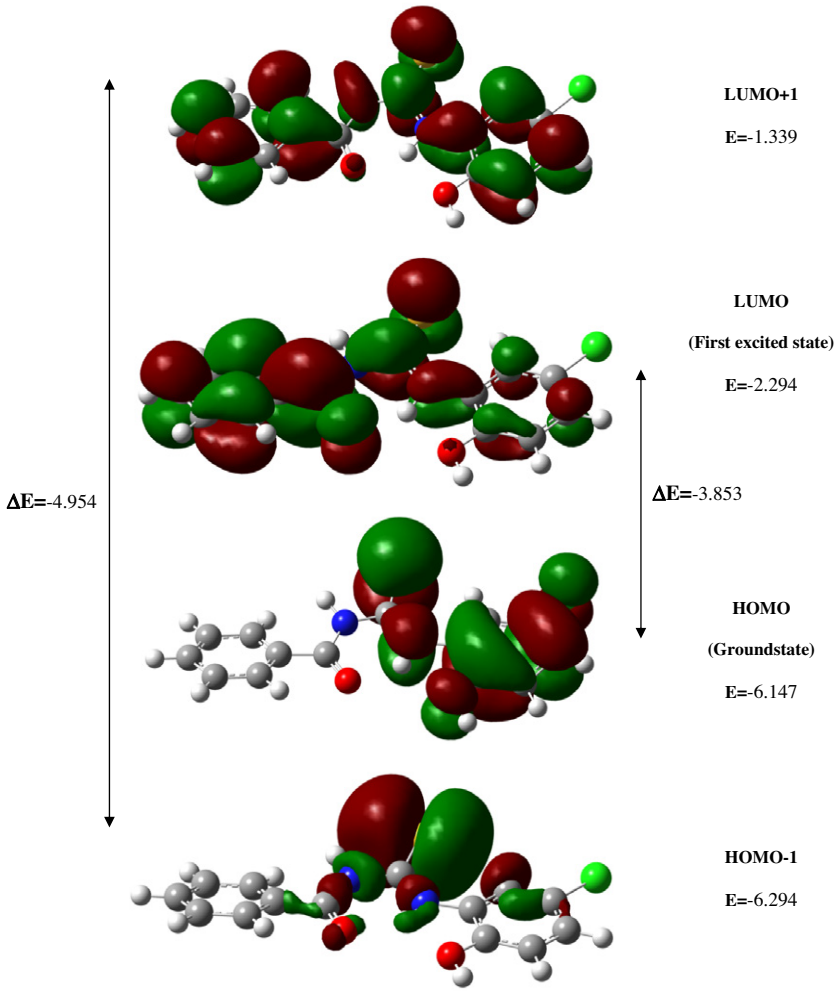

Fig. 6. The atomic orbital compositions of the frontier molecular orbital of 1-benzoyl-3-(5-chloro-2-hydroxyphenyl)thiourea (energies given in eV).

Table 6
The Experimental and theoretical electronic absorption spectra values of **bcht**.

TD-DFT/B3LYP/6-311++G(d,p)					
Solvent	Wavelengths λ (nm)		Excitation energies (eV)	Oscillator strengths (*f*)	Log ε
	Exp.	Theo.			
Acetonitrile	239	278.08	4.459 (73,75,78→80;78→81)	0.13	4.36
	266	280.84	4.415 (76→80,79→81)	0.61	4.26
	328	352.23	3.520 (79→80)	0.21	3.95
Methanol	240	279.23	4.440 (76,77→80; 79→81)	0.13	4.26
	263	280.74	4.416 (76→80; 79→81)	0.61	4.20
	331	352.13	3.521 (79→80)	0.21	3.90

strengths are tabulated in Table 6. Experimental UV–Vis spectrum in ACN solvent is shown in Fig. 7. For ACN solvent, the three intense calculated electronic transitions at λ_{max} = 278.08 nm, f = 0.13; λ_{max} = 280.84 nm, f = 0.61 and λ_{max} = 352.23 nm, f = 0.21 have been obtained which corresponds to the experimental λ_{max} values at 239, 266 and 328 nm, respectively. For methanol solvent, the theoretical and experimental values nearly same with ACN solvent. Table 6 indicates that the theoretical transition peaks for **bcht** in both solvent are red-shifted compared with the experimental data. However, the agreement between theoretical and experimental data is acceptable.

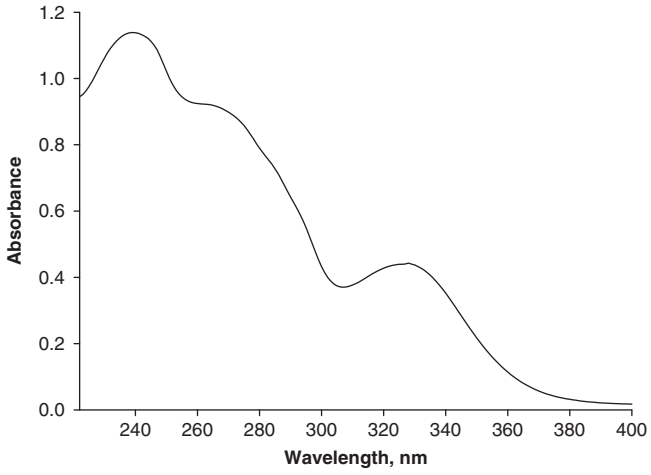

Fig. 7. The experimental UV spectrum of study compound (in ACN).

Antimicrobial activities

The in vitro antimicrobial properties against Gram positive and Gram negative bacteria, and yeast of **bcht** are presented in Table 7, respectively. **Bcht** showed different degrees of antimicrobial activity in relation to the tested species. Among the tested microorganisms, *L. monocytogenes* and *S. aureus* appears to be the most

Table 7
MIC values ($\mu g\ mL^{-1}$) of the **bcht** against the tested bacterias.

	S. aureus	*MRSA*	*S. pneumoniae*	*B. cereus*	*E. faecalis*	*L. monocytogenes*	*S. typhi*	*C. albicans*
Bcht	128	>1024	>1024	>1024	>1024	128	>1024	>1024
Vancomycine	2	2	2	4	4	2	–	–
Ciprofloxcacin	–	–	–	–	–	4	<0.25	–
Amphotericin B	–	–	–	–	–	–	–	0.25

sensitive strains MIC values of 128 $\mu g\ mL^{-1}$. However, **bcht** were inactive against the other microorganisms.

According to the antibacterial studies, the efficacy against Gram positive bacteria is higher than against Gram negative bacteria. The lower anti-yeast efficacy of the compound may be due to the differences between the cell structures of bacteria and yeast. While the cell walls of fungi contain chitin, the cell walls of bacteria contain murein [67].

Conclusions

In this work, we have synthesized a new thiourea derivative, 1-benzoyl-3-(5-chloro-2-hydroxyphenyl) thiourea and characterized by elemental analyses, FT-IR, ^{13}C, ^{1}H NMR spectroscopy. The crystal and molecular structure of **bcht** have been determined from single crystal X-ray diffraction data. We have also calculated the geometric parameters, vibrational frequencies and NMR spectroscopy of **bcht** by using the B3LYP method with the standard 6-311++G(d,p) basis sets. We have used the scaling factor values of 0.9879 for DFT/6-311++G (d,p) in order to fit the theoretical bond lengths with the experimental ones. Scaling factors results seemed to be in a better agreement with the experimental ones. The difference between experimental and calculated geometrical parameters and vibration mode can come from the difference of the state. In fact, it is evident gas state vibration frequencies are larger than those of solid state. Moreover, solid states of the compound include a lot of intra- and inter-molecular interactions. The experimental and theoretical chemical shift results are generally in good agreement. However, all of the theoretical ^{13}C NMR values a bit bigger from observed values. But in ^{1}H NMR values, there is not any systematic relation between experimental and calculated values. The electronic properties were also calculated and experimental electronic spectrum was recorded with helping of UV–Vis spectrometer. The theoretical electronic transition peaks for **bcht** in ACN and MeOH solvent are red-shifted compared with the experimental data. In general, it is seen acceptable agreement between experimental and theoretical data. **Bcht** exhibited antimicrobial activity against, *L. monocytogenes* and *S. aureus.*

Acknowledgements

This work supported by Nevşehir University Scientific Research Projects Unit (BAP, Project No.: 2011/14). We also thank Assoc. Prof. Dr. Osman CANKO for Gaussian 09 calculation performed at Erciyes University, Kayseri, Turkey.

Appendix A. Supplementary data

Crystallographic data (excluding structure factors) have been deposited with the Cambridge Crystallographic Data Centre as the supplementary publication No. CCDC 878345. A copy of the data can be obtained, free of charge, on application to CCDC, 12 Union Road, Cambridge CB21EZ, UK (fax: +44 1223 336033 or e-mail: deposit@ccdc.cam.ac.uk).

References

[1] D.G. Patil, M.R. Chedekel, J. Org. Chem. 49 (1984) 997–1000.
[2] N. Bailey, A.W. Dean, D.B. Judd, D. Middlemiss, R. Storer, S.P. Watson, Bioorg. Med. Chem. Lett. 6 (1996) 1409–1414.
[3] H. Ghosh, Synlett (2009) 2882–2883.
[4] M.K. Rauf, M. Ebihara, A. Badshah, Imtiaz-ud-Din, Acta Crystallogr. E 68 (2012) o119.
[5] W. Henderson, R.D.W. Kemmitt, S. Mason, M.R. Moore, J. Fawcett, D.R. Russell, Dalton Trans. (1992) 59–66.
[6] M. Lipowska, B.L. Hayes, L. Hansen, A. Taylor, L.G. Marzilli, Inorg. Chem. 35 (1996) 4227–4231.
[7] C. Sacht, M.S. Datt, S. Otto, A. Roodt, Dalton Trans. (2000) 4579–4586.
[8] J.H. Hu, X.H. Fan, X.L. Du, T.B. Wei, Phosphorus Sulfur 185 (2010) 2558–2562.
[9] M. Merdivan, F. Karipcin, N. Kulcu, R.S. Aygun, J. Therm. Anal. Calorim. 58 (1999) 551–557.
[10] G. Binzet, H. Arslan, U. Florke, N. Kulcu, N. Duran, J. Coord. Chem. 59 (2006) 1395–1406.
[11] D.S. Mansuroglu, H. Arslan, U. Florke, N. Kulcu, J. Coord. Chem. 61 (2008) 3134–3146.
[12] Y.F. Yuan, J.T. Wang, M.C. Gimeno, A. Laguna, P.G. Jones, Inorg. Chim. Acta 324 (2001) 309–317.
[13] B.K. Kaymakcioglu, S. Rollas, E. Korcegez, F. Aricioglu, Eur. J. Pharm. Sci. 26 (2005) 97–103.
[14] B.K. Venkatesh, Y.D. Bodke, S.A. Biradar, Phosphorus Sulfur 185 (2010) 1926–1931.
[15] S. Saeed, N. Rashid, P.G. Jones, M. Ali, R. Hussain, Eur. J. Med. Chem. 45 (2010) 1323–1331.
[16] G.Y. Sarkis, E.D. Faisal, J. Heterocycl. Chem. 22 (1985) 137–140.
[17] Z. Zhong, R. Xing, S. Liu, L. Wang, S.B. Cai, P.C. Li, Carbohyd. Res. 343 (2008) 566–570.
[18] S. Saeed, N. Rashid, P.G. Jones, R. Hussain, M.H. Bhatti, Cent. Eur. J. Chem. 8 (2010) 550–558.
[19] S. Nishizawa, R. Kato, T. Hayashita, N. Teramae, Anal. Sci. 14 (1998) 595–597.
[20] L.S. Evans, P.A. Gale, M.E. Light, R. Quesada, New J. Chem. 30 (2006) 1019–1025.
[21] J.N. Babu, V. Bhalla, M. Kumar, R.K. Puri, R.K. Mahajan, New J. Chem. 33 (2009) 675–681.
[22] V. Blazek, N. Bregovic, K. Mlinaric-Majerski, N. Basaric, Tetrahedron 67 (2011) 3846–3857.
[23] Y. Sohtome, Y. Hashimoto, K. Nagasawa, Adv. Synth. Catal. 347 (2005) 1643–1648.
[24] Y.B. Huang, C. Cai, J. Chem. Res.Sci. (2009) 686–688.
[25] W. Huang, C. Peng, L. Guo, R. Hu, B. Han, Synlett (2011) 2981–2984.
[26] J. Alonso-Chamarro, Perkin Trans. (2001) 2211–2218.
[27] D. Wilson, M.D. Arada, S. Alegret, M. del Valle, J. Hazard. Mater. 181 (2010) 140–146.
[28] A. Dago, M.A. Simonov, E.A. Pobedimskaya, A. Martin, A. Masias, Kristallografiya 33 (1988) 1021–1023.
[29] V.K. Madan, A.D. Taneja, V.P. Kudesia, J. Indian Chem. Soc. 68 (1991) 471–472.
[30] W.Q. Zhou, J.M. Lu, Z.J. Zhang, Y. Zhang, Y. Cao, L. Lu, X.J. Yang, Vib. Spectrosc. 34 (2004) 199–204.
[31] B.M. Yamin, U.M. Osman, Acta Crystallogr. E 67 (2011) O1286–U1684.
[32] W. Yang, W.Q. Zhou, Z.J. Zhang, J. Mol. Struct. 828 (2007) 46–53.
[33] H. Arslan, U. Florke, N. Kulcu, G. Binzet, Spectrochim. Acta A 68 (2007) 1347–1355.
[34] M.J. Frisch, G.W. Trucks, H.B. Schlegel, G.E. Scuseria, M.A. Robb, J.R. Cheeseman, G. Scalmani, V. Barone, B. Mennucci, G.A. Petersson, H. Nakatsuji, M. Caricato, X. Li, H.P. Hratchian, A.F. Izmaylov, J. Bloino, G. Zheng, J.L. Sonnenberg, M. Hada, M. Ehara, K. Toyota, R. Fukuda, J. Hasegawa, M. Ishida, T. Nakajima, Y. Honda, O. Kitao, H. Nakai, T. Vreven, J.A. Montgomery Jr., J.E. Peralta, F. Ogliaro, M. Bearpark, J.J. Heyd, E. Brothers, K.N. Kudin, V.N. Staroverov, R. Kobayashi, J. Normand, K. Raghavachari, A. Rendell, J.C. Burant, S.S. Iyengar, J. Tomasi, M. Cossi, N. Rega, J.M. Millam, M. Klene, J.E. Knox, J.B. Cross, V. Bakken, C. Adamo, J. Jaramillo, R. Gomperts, R.E. Stratmann, O. Yazyev, A.J. Austin, R. Cammi, C. Pomelli, J.W. Ochterski, R.L. Martin, K. Morokuma, V.G. Zakrzewski, G.A. Voth, P. Salvador, J.J. Dannenberg, S. Dapprich, A.D. Daniels, Ö. Farkas, J.B. Foresman, J.V. Ortiz, J. Cioslowski, D.J. Fox, Gaussian 09, Revision B.01, Gaussian Inc., Wallingford, CT, 2009.
[35] O.V. Dolomanov, L.J. Bourhis, R.J. Gildea, J.A.K. Howard, H. Puschmann, OLEX2: a complete structure solution, refinement and analysis program, J. Appl. Cryst. 42 (2009) 339–341.
[36] G.M. Sheldrick, Acta Cryst. SHELXS A64 (2008) 112–122.
[37] G.M. Sheldrick, Acta Cryst. SHELXL A64 (2008) 112–122.

[38] M.H. Jamróz, Vibrational Energy Distribution Analysis, VEDA 4 Computer Program, Poland, 2004.
[39] R. Ditchfield, J. Chem. Phys. 56 (1972) 5688–5691.
[40] K. Wolinski, J.F. Hinton, P. Pulay, J. Am. Chem. Soc. 112 (1990) 8251–8260.
[41] Clinical and Laboratory Standards Institute (CLSI) Methods of dilution antimicrobialsusceptibility tests for bacteria that grow aerobically. Approved standard, 7th ed., CLSI, Wayne, (2006) pp. M7–A7.
[42] National Committee for Clinical Laboratory Standards. Reference method for broth dilution antifungal susceptibility testing of yeasts. Approved standard, 2nd ed., NCCLS, Wayne, (2002) pp. M27–A2.
[43] M.S. Yusof, R.H. Jusoh, W.M. Khairul, M.Y. Bohari, J. Mol. Struct. 975 (2010) 280–284.
[44] C.K. Ozer, H. Arslan, D. vanDerveer, N. Kulcu, Molecules 14 (2009) 655–666.
[45] H. Arslan, U. Flörke, N. Külcü, G. Binzet, Spectrochimica. Acta, Part A 68 (2007) 1347–1355.
[46] N. Sundaraganesan, S. Ilakiamani, H. Saleem, P.M. Wojciechowski, D. Michalska, Spectrochim. Acta, Part A 61 (2005) 2995–3001.
[47] M. Silverstein, G. Clyton Basseler, C. Morill, Spectrometric Identification of Organic Compounds, Wiley, NewYork, 1981.
[48] S. Subashchandrabose, H. Saleem, Y. Erdogdu, G. Rajarajanc, V. Thanikachalam, Spectrochim. Acta, Part A 82 (2011) 260–269.
[49] D. Dolega, A. Migal-Mikuli, J. Chrusciel, J. Mol. Struct. 933 (2009) 30–37.
[50] K. Druzbicki, E. Mikuli, M.D. Ossowska-Chrusciel, Vib. Spectrosc. 52 (2010) 54–62.
[51] N.P.G. Roeges, A Guide to the Complete Interpretation of Infrared Spectra of Organic Structures, Wiley, NewYork, 1994.
[52] G. Varsanyi, Assignments for Vibrational Spectra of Seven Hundred Benzene Derivatives, vol. 1–2, Academic Kiado: Budapest, 1973.
[53] T. Shimanouchi, Y. Kakiuti, I. Gamo, J. Chem. Phys. 25 (1956) 1245–1252.
[54] T.D. Klots, R.D. Chirico, W.V. Steele, Spectrochim. Acta, Part A 50 (1994) 765–795.
[55] D.K. Singh, S.K. Srivastava, A.K. Ojha, B.P. Asthana, J. Mol. Struct. 892 (2008) 384–391.
[56] N.M. Hosny, M.M. Mostafa, J. Inc, Phenom. Macro. 67 (2010) 85–90.
[57] F. Aydin, H. Unver, D. Aytac, N. Ocak Iskeleli, J. Chem. Cyristallogr. 40 (2010) 1082–1086.
[58] J.R. Cheeseman, G.W. Trucks, T.A. Keith, M.J. Frisch, J. Chem. Phys. 104 (1996) 5497–5509.
[59] D.R. Kelman, K.A. Claborn, W. Kaminsky, K.I. Goldberg, D.X. West, J. Mol. Struct. 642 (2002) 119–127.
[60] C. Reichardt, Solvent and Solvent Effects in Organic Chemistry, second ed., VCH, Weinheim, 1988.
[61] A. Tadjarod, F. Adhami, Y. Hanifehpour, M. Yazdi, Z. Moghaddamfard, G. Kickelbick, Polyhedron 26 (2007) 4609–4618.
[62] I. Fleming, Frontier Orbitals and Organic Chemical Reactions, Wiley, London, 1976.
[63] S. Gunasekaran, R.A. Balaji, S. Kumeresan, G. Anand, S. Srinivasan, Can. J. Anal. Sci. Spectrosc. 53 (2008) 149–162.
[64] E. Kavitha, N. Sundaraganesan, S. Sebastian, M. Kurt, Spectrochim. Acta, Part A 77 (2010) 612–619.
[65] M.M. Kumari, P.I. Ramachandra, C. Ravikumar, I.H. Joe, I. Nemec, J. Raman Spectrosc. 42 (2011) 1462–1469.
[66] R. Vivas-Reyes, E. Espinosa-Fuentes, J. Forigua, A. Arias, R. Gaitan, E. Arguello, J. Mol. Struc. Theochem 862 (2008) 92–97.
[67] M. Eweis, S.S. Elkholy, M.Z. Elsabee, Int. J. Biol. Macromol. 38 (2006) 1.